applied sciences

MDPI

Article

Green Scalar Function Method for Analyzing Dielectric Media

J. C. Bravo [1,2,*], J. Colomina-Martínez [1,2], J. J. Sirvent-Verdú [1,2], E. J. Mena [1,2], M. L. Álvarez [1,2], J. Francés [1,2], C. Neipp [1,2] and Sergi Gallego [1,2]

[1] I.U. Fisica Aplicada a las Ciencias y las Tecnologías, University of Alicante, 03080 Alicante, Spain; jaume.colomina@ua.es (J.C.-M.); jj.sirvent@ua.es (J.J.S.-V.); emilio.mena@ua.es (E.J.M.); mariela.alvarez@ua.es (M.L.Á.); jfmonllor@ua.es (J.F.); cristian@ua.es (C.N.); sergi.gallego@ua.es (S.G.)
[2] Departament de Fisica, Enginyeria de Sistemes i Teoria del Senyal, Universitat d'Alacant, 03080 Alicante, Spain
* Correspondence: juanc.bravo@ua.es

Abstract: In this work we present a formalism based on scalar Green's functions to deal with electromagnetic scattering problems. Although the formulations of the Mie theory and Born approximations in terms of electromagnetic scattering are well known and relevant, they have certain disadvantages: complexity, computational time, few symmetries, etc. Therefore, the study with scalar Green's functions allows dealing with these problems with greater simplicity and efficiency. However, the information provided by the vector formulation is sacrificed. Nevertheless, different cases of electromagnetic scattering of dielectric media with different dimensions, geometries and refractive indices will be presented. Thus, we will be able to verify the capacity of this scalar method in predicting light-scattering problems.

Keywords: Green functions; scattering; dielectric media; diffraction

check for updates

Citation: Bravo, J.C.; Colomina-Martínez, J.; Sirvent-Verdú, J.J.; Mena, E.J.; Álvarez, M.L.; Francés, J.; Neipp, C.; Gallego, S. Green Scalar Function Method for Analyzing Dielectric Media. *Appl. Sci.* **2024**, *14*, 8045. https://doi.org/10.3390/app14178045

Received: 6 August 2024
Revised: 2 September 2024
Accepted: 4 September 2024
Published: 8 September 2024

1. Introduction

Scattering problems are of great importance in applications such as optical device design [1], medical imaging [2], object detection [3,4] and materials science. Theories such as the Mie theory [5,6], the Born approximation [7] and advanced numerical methods are essential tools for tackling these problems [8–11]. Some of these methods consist of solving time-dependent Maxwell's equations [12,13], obtaining Mie's coefficients [14], employing method of moments (MoM) or the Galerkin method [15,16]. However, these theories have certain disadvantages such as complex and computationally expensive calculations, application to regular surfaces, lack of accuracy with high dielectric constant or small dimensions, hard dicretization of the equations, etc. [17–20]. Therefore, in the present work, a scalar formalism with Green's functions [21–23] is shown. These show the impulsional response of a linear system. Specifically, in the electromagnetic domain, an impulsional response represents a point source in space as if it were a Dirac delta. This makes it possible to describe the electric and magnetic fields and their potentials in terms of these point sources. This allows us to know the distribution of the reflected, refracted and scattered fields. On the other hand, the scalar formulation allows us greater computational efficiency and the possibility of contrasting this methodology with different scattering cases where an analytical solution is presented. Moreover, scalar methods are particularly applicable in the analysis of scattering in homogeneous media (or those in which the refractive index varies slowly over the thickness) and in the characterization of materials through techniques such as spectroscopy [24]. To this end, the Helmholtz equation will be derived from Maxwell's equations, and the solution of this equation will be posed in terms of the scalar Green's functions. In some cases, due to the symmetry of the problem, the dimensionality can be simplified. In the following, different geometries will be presented in order to analyze the resulting electromagnetic scattering, varying the system's own parameters such as dimensions and refractive index.

2. Theoretical Background

The Green's function applied to the Helmholtz equation is the solution of the wave equation for a point source. Thus, if the solution for this point source is known, then the solution for a general source can be obtained by the superposition principle. This result follows from the linearity of the wave equation itself, since any source can be described by the linear superposition of point sources. For our case, we will consider a scalar field $E(\boldsymbol{r})$, which has a source $s(\boldsymbol{r})$. The Helmholtz equation associated with this system would be

$$(\nabla^2 + k^2)E(\boldsymbol{r}) = s(\boldsymbol{r}) \tag{1}$$

and using the definition of Green's scalar function, now renamed $g(\boldsymbol{r}, \boldsymbol{r'})$, we have that

$$\left(\nabla^2 + k^2\right)g(\boldsymbol{r}, \boldsymbol{r'}) = -\delta(\boldsymbol{r} - \boldsymbol{r'}) \tag{2}$$

Thus, we can establish a relationship between (1) and (2) as

$$E(\boldsymbol{r}) = -\int_V g(\boldsymbol{r}, \boldsymbol{r'})s(\boldsymbol{r'})d\boldsymbol{r'} \tag{3}$$

This solution will only depend on $R = |\boldsymbol{r} - \boldsymbol{r'}|$ and in general could be written as

$$g_{3D}(\boldsymbol{r}, \boldsymbol{r'}) = g(\boldsymbol{r} - \boldsymbol{r'}) = \frac{e^{ik|\boldsymbol{r}-\boldsymbol{r'}|}}{4\pi|\boldsymbol{r} - \boldsymbol{r'}|} = \frac{e^{ikR}}{4\pi R} \tag{4}$$

Given the Equations (3) and (4), we can write the scalar field associated with such a source as

$$E(\boldsymbol{r}) = -\int_V \frac{e^{ik|\boldsymbol{r}-\boldsymbol{r'}|}}{4\pi|\boldsymbol{r} - \boldsymbol{r'}|}s(\boldsymbol{r'})d\boldsymbol{r'} \tag{5}$$

2.1. 2D Green Function

As in 3D systems, the scalar Green's function in 2D geometries will only depend on the relative position between the source and the observer, so it is convenient to define the relative coordinates.

$$\boldsymbol{r} - \boldsymbol{r'} \equiv \boldsymbol{\rho} - \boldsymbol{\rho'} = (\rho\cos\phi, \rho\sin\phi, 0) = (x - x', y - y', z - z') \tag{6}$$

Thus, it is reducing the three-dimensional problem to one in the plane. In the 3D case, the scalar Green's function refers to a point source of electromagnetic fields, which are located in $(x', y', z') = (0, 0, z')$. However, the 2D case refers to the field generated by an infinite linear charge source observed in a plane $z =$ const. whose axial dependence for with the term $\exp(ik_z z)$. So, one can obtain this 2D Green's function, $g_{2D}(\boldsymbol{r}, \boldsymbol{r'})$, as the line integral of this linear source

$$g_{2D}(\boldsymbol{r}, \boldsymbol{r'}) = \int_{-\infty}^{\infty} g_{3D}(\boldsymbol{r}, \boldsymbol{r'})e^{ik_z z'}dz' = \int_{-\infty}^{\infty} \frac{e^{ik\sqrt{x^2+y^2+(z-z')^2}}}{4\pi\sqrt{x^2 + y^2 + (z - z')^2}}e^{ik_z z'}dz' = -\frac{i}{4}H_0(k_\rho\rho)e^{ik_z z} \tag{7}$$

where $H_0(k_\rho\rho)$ denotes the Hankel function of the first kind, $k = |\boldsymbol{k}| = |(\boldsymbol{k_\rho}, k_z)|$ is the wave vector modulus, and $k_\rho = |\boldsymbol{k_\rho}|$ is the transverse wave vector modulus, respectively.

2.2. Discretization of the Equations

Consider the Helmholtz scalar equation applied to the electric field and applied to a Green scalar function

$$\nabla^2 E(\boldsymbol{r}) + k_0^2\varepsilon_B E(\boldsymbol{r}) = -k_0^2\Delta\varepsilon(\boldsymbol{r})E(\boldsymbol{r}) \tag{8}$$

$$\left(\nabla^2 + k_0^2\varepsilon_B\right)g(\boldsymbol{r}, \boldsymbol{r'}) = -\delta(\boldsymbol{r}, \boldsymbol{r'}) \tag{9}$$

where $\Delta\varepsilon(\boldsymbol{r}) = \varepsilon(\boldsymbol{r}) - \varepsilon_B$ is the dielectric contrast, indicating the difference in dielectric permittivity between the object $\varepsilon(\boldsymbol{r})$ and the background ε_B. The procedure followed to

obtain the scattered pattern is analogous to the one described in Section II.A of [25] except that we address the scalar case. On the other hand, if we introduce Equation (9) into Equation (8), electric field $E(\boldsymbol{r})$ can be obtained by

$$E(\boldsymbol{r}) = E^{(1)}(\boldsymbol{r}) + \int_V g(\boldsymbol{r}, \boldsymbol{r}') \cdot k_0^2 \Delta\varepsilon(\boldsymbol{r}') E(\boldsymbol{r}') d\boldsymbol{r}' \tag{10}$$

where the integration is calculated over the whole volume of the chosen simulated region and $E^{(1)}(\boldsymbol{r})$ refers to the incident electric field. The circumstance to be solved that may arise in the study of a reduced volume is the singularity $|\boldsymbol{r} - \boldsymbol{r}'| \to 0$. Therefore, when $\boldsymbol{r} \approx \boldsymbol{r}'$, the singularity can be avoided if we exclude that infinitesimal element of volume δV where this singularity is found. We can then treat this singularity separately, rewriting Equation (10) as

$$E(\boldsymbol{r}) = E^{(1)}(\boldsymbol{r}) + \lim_{\delta V \to 0} \int_{V - \delta V} g(\boldsymbol{r}, \boldsymbol{r}') \cdot k_0^2 \Delta\varepsilon(\boldsymbol{r}') E(\boldsymbol{r}') d\boldsymbol{r}' - L \cdot \frac{\Delta\varepsilon(\boldsymbol{r})}{\varepsilon_B} E(\boldsymbol{r}) \tag{11}$$

where L is a scalar term derived from the dyad $\boldsymbol{L}$ [25] which depends on the geometry of the excluded volume δV. Thus, in our work, the observation point $\boldsymbol{r}$ is located outside the dispersive medium or "scatterer", whose position is given by $\boldsymbol{r}'$. To solve Equation (11) numerically, we must first define a grating of N nodes which represents the system. Each node i will be centered in a position $\boldsymbol{r}_i$ and will present a volume V_i if we are in 3D or an area in 2D and a value of dielectric contrast. Following, electric field $E_i = E(\boldsymbol{r}_i)$ must be discretized as well as scalar Green's function $g_{i,j} = g(\boldsymbol{r}_i, \boldsymbol{r}_j)$.

$$E_i = E_i^{(1)} + \sum_{\substack{j=1 \\ j \neq i}}^{N} g_{i,j} \cdot k_0^2 \Delta\varepsilon_j E_j V_j + M_i \cdot k_0^2 \Delta\varepsilon_i E_i - L \cdot \frac{\Delta\varepsilon_i}{\varepsilon_B} E_i \qquad i = 1, \ldots, N \tag{12}$$

and

$$M_i = \lim_{\delta V \to 0} \int_{V_i - \delta V} g(\boldsymbol{r}_i, \boldsymbol{r}') d\boldsymbol{r}' \tag{13}$$

Throughout the implementation of the codes and simulations, it has become clear that the terms where the scalar Green's function or the geometric factor L appears, these prevail over M_i. However, many authors for more complex geometries than the ones we will deal with in the project show that the M_i term is more relevant than the L term E_i as in [25]. Equation (12) represents a linear system of equations that can be solved with simple numerical methods. Expressing the system of equations in the form

$$E_i^{(1)} = E_i \cdot \left[1 - M_i k_0^2 \Delta\varepsilon_i + L \frac{\Delta\varepsilon_i}{\varepsilon_B}\right] - \sum_{\substack{j=1 \\ j \neq i}}^{N} g_{i,j} \cdot k_0^2 \Delta\varepsilon_j E_j V_j E_j \qquad E_i = A_G^{-1} E_i^{(1)} \tag{14}$$

where A_G is the interaction matrix which contains the scalar Green's function and the dielectric contrast and geometric factor terms of the source L, which is defined by

$$A_G(i,j) = \begin{cases} 1 - M_i k_0^2 \Delta\varepsilon_i + L \dfrac{\Delta\varepsilon_i}{\varepsilon_B} & \text{if} \quad i = j \\ -g_{i,j} k_0^2 \Delta\varepsilon_j V_j & \text{if} \quad i \neq j \end{cases} \tag{15}$$

Following our notation, E_i is the simulated electric field matrix, and $E_i^{(1)}$ is the incident field. In terms of the segmentation, this is carried out assuming that the dielectric object is composed of small circular scatterers [26]. We assign at each point a value of the dielectric constant and slightly vary the refractive index values to avoid convergence problems due to boundary conditions.

2.3. Scalar Analytical Solution

The scalar approximation simplifies the analysis of electromagnetic wave scattering by reducing the problem to a scalar field rather than dealing with the full vector nature of electromagnetic fields. This approach is especially useful when the variations in the wave field occur mainly in a single component, allowing for simpler mathematical handling and greater computational efficiency. By using scalar fields, we can take advantage of well-established mathematical techniques, such as Fourier series, to express the fields in terms of their angular harmonics. Since analytical solutions for cylindrical symmetries are studied in the literature, we opted to use cylindrical dielectric media. In order to compare the numerical results, the analytical solution presented in Section 2.1 in [27] is used. Thus, to achieve this, a homogeneous cylinder is considered to obtain the scattered field in cylindrical coordinates in terms of a Fourier series in the angular coordinate. Lets us consider an incident wave front in plane $y = 0$ parallel polarized with respect to the z-axis; thus, the electric field in cylindrical coordinates expressed as a Fourier series in the angular coordinate is given by

$$E^{(1)}(\rho, \phi) = E_0 e^{ikx} = E_0 \sum_{m=-\infty}^{\infty} i^m J_m(k\rho) e^{im\phi} \tag{16}$$

where E_0 is the amplitude of the incident wave, ϕ is the angle that the scattered wave forms with respect to the incident wave and J is the Bessel function of first kind. Once we have expressed the incident field in Fourier terms as a function of the angular harmonics, we can give the expression for the scattered field $E^{(3)}$ as

$$E^{(3)}(\rho, \phi) = E_0 e^{ik\rho\cos\phi} = E_0 \sum_{m=-\infty}^{\infty} i^m \alpha_m H_m(k\rho) e^{im\phi} \tag{17}$$

This Equation (17) satisfies the Sommerfeld radiation condition at infinity. Here, α_m is a constant describing the continuity of the dielectric field derived by the boundary conditions as obtained in [28] for a perpendicular polarization across the xz-plane, which is given by

$$\alpha_m = \frac{nJ'_m(ka)J_m(nka) - J_m(ka)J'_m(nka)}{nJ_m(nka)H'_m(ka) - J'_m(kna)H_m(ka)} \tag{18}$$

where $k = 2\pi/\lambda$ is the modulus of grating vector $\boldsymbol{k}$, n is the refractive index of the dielectric media and a is the cylinder radius. The scalar approximation provides significant insight into the scattering problem by simplifying the analysis. However, it should be noted that the solutions obtained using this scalar approximation are analogous to those derived from the full vector treatment in the case of TE (Transverse Electric) polarization. In this context, TE polarization implies that the electric field is perpendicular to the plane of incidence, making the scalar approximation of the field a valid representation of the vector field under these specific conditions, as it is described in [25].

3. Numerical Results

First, the analytical solutions obtained by the Fourier series development of the angular harmonics are compared with the scalar formalism of Green's function. In order to achieve this, consider the following coordinate scheme presented in Figure 1. When a plane wave, polarized perpendicularly, impinges on the cylinder in the xz-plane with a tilt angle ζ, the intensity pattern of the scattered light is measured on a screen. On the other hand, the screen where the intensity pattern is collected can be moved along the axial axis y, and the intensity can be gathered at different distances from the cylinder.

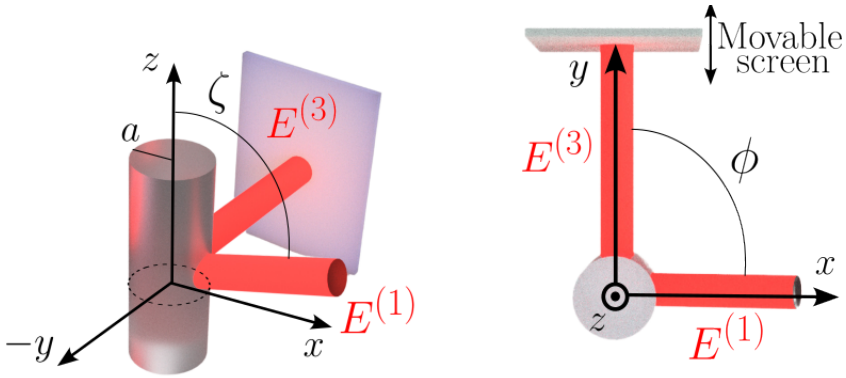

Figure 1. Coordinate system for a scattering cylinder.

In the following simulations, we can see the axial evolution of the normalized intensity of the scattered light with $\lambda = 633$ nm in Figure 2a, moving toward the screen with respect to the cylinder, and the pattern of the scattered light on the screen at a distance of $y = 10$ mm, as shown in Figure 2b. We can see that the proposed numerical method with the Green's function approximates and behaves in an analogous way to the analytical solution proposed by Equation (17). Moreover, in Figure 2a, we observe that for values close to $y = 0$, the behavior of the axial intensity curve presents some abrupt changes in the intensity, which is in agreement with the scalar theory of diffraction being in the Fresnel regime close to the source.

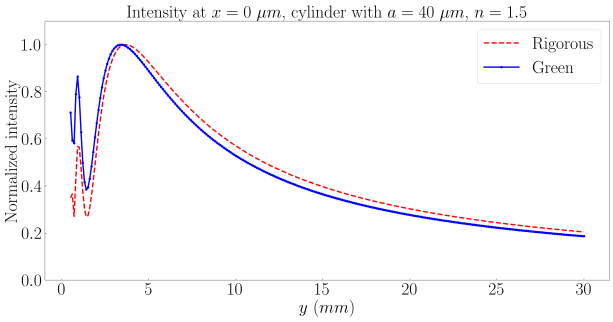

(**a**) Axial variation of intensity pattern

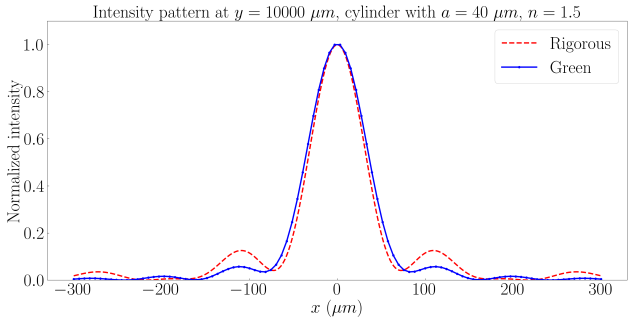

(**b**) Radial variation of intensity pattern

Figure 2. Cylinder with circular base $a = 40$ µm and with refractive index of $n = 1.5$.

Modifying the dimensions of the dielectric medium, in this case reducing its dimensions by half ($a = 20$ µm), we can observe how the pattern of the scattered beam on the screen widens with respect to the intensity pattern for a cylinder twice the size; see Figure 3b with respect to Figure 2b. This result shows that the light scattered by the dielectric medium actually has its origin in the diffraction that the cylinder itself performs when incident on light [29]. On the other hand, the axial behavior of the intensity of the scattered beam, as seen in Figure 3a, shows less variation as it approaches the source and decays faster than a larger scattering medium in comparison with Figure 2a. These two comments are consistent with the scalar theory of light diffraction. On the other hand, the solution obtained by the scalar Green's method fits the analytical solution better (17).

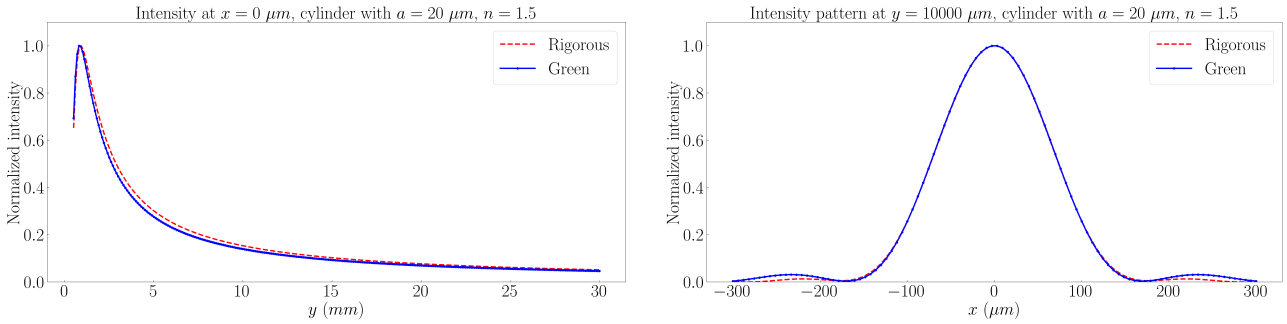

(**a**) Axial variation of intensity pattern (**b**) Radial variation of intensity pattern

Figure 3. Cylinder with circular base $a = 20$ µm and with refractive index of $n = 1.5$.

Once it has been demonstrated that the numerical method fits the analytical prediction, we decided to try different geometries and to analyze the scattered field in the plane. Thus, the following results represent the light scattering of different dielectric surfaces. For this purpose, a 2D scalar Green's function given by Equation (9) is used. In Figure 4a, we consider a cylinder with an elliptical base with a semi-major axis $a = 30$ µm and semi-minor axis $b = 10$ µm with refractive index $n = 1.5$. A planar wave front with a wavelength of $\lambda = 633$ nm propagating in air impinges normally on the dielectric surface, $\zeta = \pi/2$. We can observe the pattern of the scattered field $E^{(3)}$ once the electromagnetic wave interacts with the dielectric cylinder. It should be noted that the incident beam is on the y-axis according to the coordinate system of Figure 4. This presents two clear scattered wave fronts, which refers to the reflection of the incident wave $E^{(1)}$. On the other hand, in Figure 4b, the intensity of the refracted field inside the dielectric cylinder is represented.

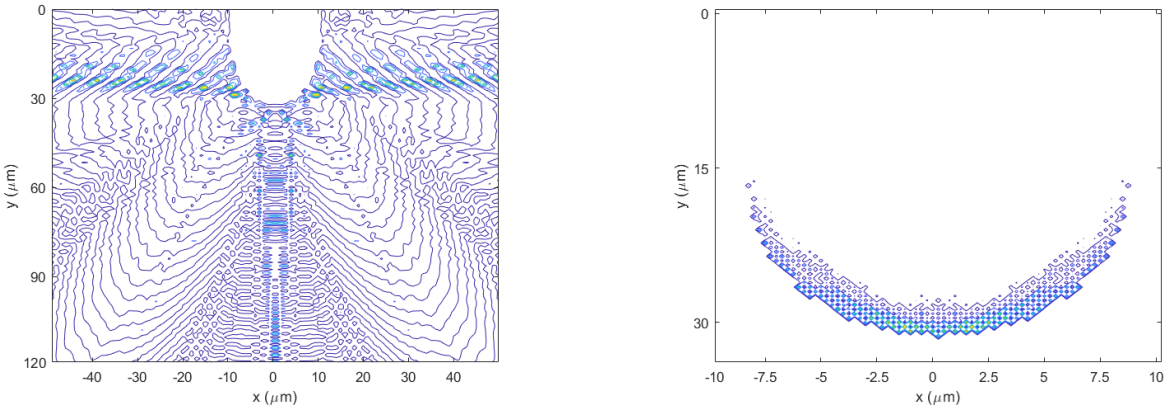

(**a**) External electric field $E^{(3)}$ (**b**) Inner electric field $E^{(2)}$

Figure 4. Cylinder with elliptical base ($a = 30$ µm and $b = 10$ µm) with refractive index of $n = 1.5$.

Trying other geometries, we opted for a prism with a rectangular base 20×30 µm^2. We have in the following Figure 5a the scattered field by this new dielectric medium for a refractive index $n = 1.5$ and the internal field for different refractive indices, $n = 1.5$ in Figure 5b and $n = 1.05$ in Figure 5c. We can observe how the homogeneity of the transmitted electromagnetic wave has a certain dependence on the difference between refractive indices of the dielectric medium with respect to the external medium; in this case, air $n = 1$. These results make sense, because the intensity of the field transmitted by the dielectric medium depends on the refractive index due to the Fresnel equations, so the greater the relative difference in refractive indices, the less electric field will be transmitted and the less scattered field there will be at the output of the dielectric medium. Furthermore, we can see how the areas of highest intensity are at the interface between

refracting surfaces, and this intensity decreases as the electric field propagates through the interior of the prism as it occurs in the dielectric cylinder. Good agreement between the scalar Green method and vector form [30,31] is observed.

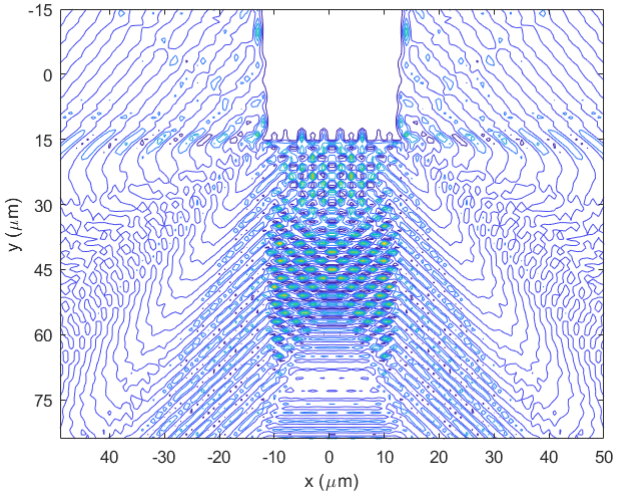

(**a**) Scattered electric field $E^{(3)}$ with $n = 1.5$

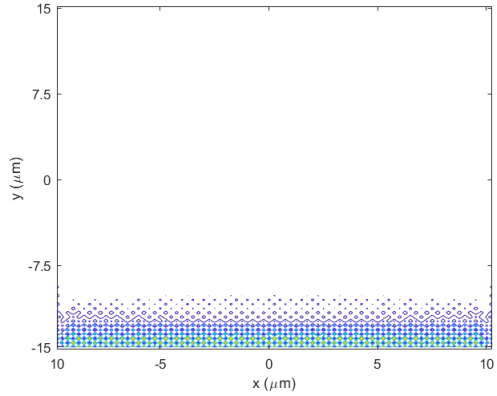

(**b**) Inner electric field $E^{(2)}$ with $n = 1.5$

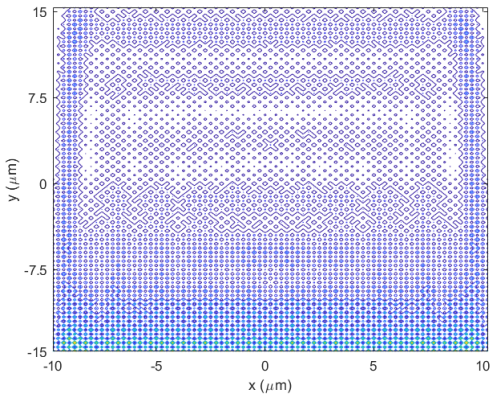

(**c**) Inner electric field $E^{(2)}$ with $n = 1.05$

Figure 5. Rectangular prism with base $a = 20$ μm, $b = 30$ μm and different refractive index.

4. Discussions

The simplicity of the equations derived from Green's functions combined with the proposed numerical method makes this approximate method a good approach to deal with electromagnetic scattering problems. The literature opts for more complex formalism and more computationally expensive resolution methods such as FDTD or commercial software such as COMSOL, HFSS... However, the methodology presented in this work allows to reduce the computational costs by reducing the size of the electric field matrices and therefore the execution time due to the scalar formalism employing Matlab software. Moreover, this numerical method has been compared with other analytical solutions proposed in the literature, and it has been found to fit properly. In addition, phenomena such as light diffraction have been verified by modifying the dimensions of the selected dielectric element, which in this work is a homogeneous cylinder. Thus, a distinction between Figures 2 and 3 is the size of the dielectric cylinder. Figure 2 features a cylinder with a radius twice that of Figure 3. This difference in dimensions leads to variations in the diffraction patterns. As expected, the larger cylinder in Figure 2 exhibits a more complex interference pattern due to the increased number of available scattering modes and finer subdivision of Fresnel zones. Consequently, the axial representation in Figure 2a

shows pronounced peaks, reflecting the influence of the dimensionality factor in the matrix equation. In contrast, Figure 3a presents a smoother profile, more closely resembling the analytical result, which is likely attributed to the reduced size and its corresponding impact on the system of equations. Another aspect shown is the transmission of light through a dielectric medium.

5. Conclusions

To sum up, we can say that Green's method makes it possible to recreate the phenomena of both diffraction and refraction of light. The results highlight the effectiveness of this approach, particularly in simpler setups, by providing accurate predictions with less computational complexity. On the other hand, future research will be carried out to study more complex geometries or inhomogeneous dielectric media. However, as it is a scalar method, information about the degree of polarization of the scattered field is missed. This aspect could be addressed with a vectorial numerical method based on a tensor formalism with Green's functions.

Author Contributions: Following the taxonomy of CRediT, the contributions of each author are as follows: J.C.B. contributed to the conceptualization, formal analysis, investigation, methodology, resources, software development, data curation, visualization, and writing of the original draft as well as the review and editing of the manuscript. J.C.-M. managed the formal analysis, investigation, software development and data curation. J.J.S.-V. colaborated on the formal analysis, investigation, software development and data curation. E.J.M. assisted with the investigation and visualization. M.L.Á. took part in the formal analysis, investigation and visualization. J.F. supported regarding the resources, software development, data curation and visualization. C.N. was involved in project administration, conceptualization, investigation, resources, software development, supervision, validation, and visualization. S.G. was responsible for funding acquisition, project administration, conceptualization, investigation, methodology, resources, supervision, validation, and visualization. All authors have read and agreed to the published version of the manuscript.

Funding: Funded by the "Generalitat Valenciana" (Spain) (IDIFEDER/2021/014, cofunded by EU through FEDER Programme; PROMETEO/2021/006 and INVEST/2022/419 financed by Next Generation EU), "Ministerio de Ciencia e Innovación" (Spain) (PID2021-123124OB-I00 and PID2019-106601RB-I00).

Institutional Review Board Statement: Not applicable.

Informed Consent Statement: Not applicable.

Data Availability Statement: The original contributions presented in the study are included in the article, further inquiries can be directed to the corresponding author.

Conflicts of Interest: The authors declare that they have no known competing financial interests or personal relationships that could have appeared to influence the work reported in this paper.

References

1. Stefanou, N.; Karathanos, V.; Modinos, A. Scattering of electromagnetic waves by periodic structures. *J. Phys. Condens. Matter* **1992**, *4*, 7389. [CrossRef]
2. Rekanos, I.T. Neural-network-based inverse-scattering technique for online microwave medical imaging. *IEEE Trans. Magn.* **2002**, *38*, 1061–1064. [CrossRef]
3. Doicu, A.; Wriedt, T.; Eremin, Y.A. *Light Scattering by Systems of Particles: Null-Field Method with Discrete Sources: Theory and Programs*; Springer: Berlin/Heidelberg, Germany, 2006; Volume 124.
4. Bohren, C.F.; Huffman, D.R. *Absorption and Scattering of Light by Small Particles*; John Wiley & Sons: Hoboken, NJ, USA, 2008.
5. Nieto-Vesperinas, M. Fundamentals of Mie scattering. In *Dielectric Metamaterials*; Elsevier: Amsterdam, The Netherlands, 2020; pp. 39–72.
6. Zhang, S.; Zhang, W.; Liu, L. Light scattering by a charged infinite cylinder in a transparent medium. *J. Quant. Spectrosc. Radiat. Transf.* **2020**, *253*, 107167. [CrossRef]
7. Habashy, T.M.; Groom, R.W.; Spies, B.R. Beyond the Born and Rytov approximations: A nonlinear approach to electromagnetic scattering. *J. Geophys. Res. Solid Earth* **1993**, *98*, 1759–1775. [CrossRef]
8. Rao, S.; Wilton, D.; Glisson, A. Electromagnetic scattering by surfaces of arbitrary shape. *IEEE Trans. Antennas Propag.* **1982**, *30*, 409–418. [CrossRef]

9. Rother, T. Self-consistent Green's function formalism for acoustic and light scattering, Part 1: Scalar notation. *Opt. Commun.* **2005**, *251*, 254–269. [CrossRef]
10. Ishimaru, A. *Electromagnetic Wave Propagation, Radiation, and Scattering: From Fundamentals to Applications*; John Wiley & Sons: Hoboken, NJ, USA, 2017.
11. Kahnert, F.M. Numerical methods in electromagnetic scattering theory. *J. Quant. Spectrosc. Radiat. Transf.* **2003**, *79*, 775–824. [CrossRef]
12. Taflove, A.; Brodwin, M.E. Numerical solution of steady-state electromagnetic scattering problems using the time-dependent Maxwell's equations. *IEEE Trans. Microw. Theory Tech.* **1975**, *23*, 623–630. [CrossRef]
13. Nick, J.; Kovács, B.; Lubich, C. Time-dependent electromagnetic scattering from thin layers. *Numer. Math.* **2022**, *150*, 1123–1164. [CrossRef]
14. Shah, G.A. Numerical methods for Mie theory of scattering by a sphere. *Kodalkenel Obs. Bull. Ser. A* **1977**, *2*, 42–63.
15. Alyones, S.; Bruce, C.W.; Buin, A.K. Numerical methods for solving the problem of electromagnetic scattering by a thin finite conducting wire. *IEEE Trans. Antennas Propag.* **2007**, *55*, 1856–1861. [CrossRef]
16. Liu, R.Q.; Huang, X.W.; Du, Y.L.; Yang, M.L.; Sheng, X.Q. Massively parallel discontinuous Galerkin surface integral equation method for solving large-scale electromagnetic scattering problems. *IEEE Trans. Antennas Propag.* **2021**, *69*, 6122–6127. [CrossRef]
17. Glisson, A.; Wilton, D. Simple and efficient numerical methods for problems of electromagnetic radiation and scattering from surfaces. *IEEE Trans. Antennas Propag.* **1980**, *28*, 593–603. [CrossRef]
18. Sevgi, L. *Complex Electromagnetic Problems and Numerical Simulation Approaches*; John Wiley & Sons: Hoboken, NJ, USA, 2003.
19. Paknys, R. *Applied Frequency-Domain Electromagnetics*; John Wiley & Sons: Hoboken, NJ, USA, 2016.
20. Wubs, M.; Suttorp, L.; Lagendijk, A. Multiple-scattering approach to interatomic interactions and superradiance in inhomogeneous dielectrics. *Phys. Rev. A-At. Mol. Opt. Phys.* **2004**, *70*, 053823. [CrossRef]
21. Huang, J.; Yao, J.; Xu, D.; Li, R. Green function method for the time domain simulation of pulse propagation. *Appl. Opt.* **2014**, *53*, 3533–3539. [CrossRef] [PubMed]
22. Huang, J. Green Function. In *Perturbation Theory*; Uzunov, D.I., Ed.; IntechOpen: Rijeka, Croatia, 2017; Chapter 3. [CrossRef]
23. Bevacqua, M.T.; Isernia, T. An effective rewriting of the inverse scattering equations via Green's function decomposition. *IEEE Trans. Antennas Propag.* **2021**, *69*, 4883–4893. [CrossRef]
24. Born, M.; Wolf, E. *Principles of Optics: Electromagnetic Theory of Propagation, Interference and Diffraction of Light*; Elsevier: Amsterdam, The Netherlands, 2013.
25. Martin, O.J.; Piller, N.B. Electromagnetic scattering in polarizable backgrounds. *Phys. Rev. E* **1998**, *58*, 3909–3915. [CrossRef]
26. Taleb, S.I.; Neipp, C.; Francés, J.; Márquez, A.; Alvarez, M.L.; Hernández, A.; Gallego, S.; Beléndez, A. Validation of Fresnel–Kirchhoff Integral Method for the Study of Volume Dielectric Bodies. *Appl. Sci.* **2021**, *11*, 3800. [CrossRef]
27. Petropoulos, P.G. Reflectionless sponge layers as absorbing boundary conditions for the numerical solution of Maxwell equations in rectangular, cylindrical, and spherical coordinates. *SIAM J. Appl. Math.* **2000**, *60*, 1037–1058. [CrossRef]
28. Frezza, F.; Mangini, F.; Tedeschi, N. Introduction to electromagnetic scattering: Tutorial. *JOSA A* **2018**, *35*, 163–173. [CrossRef]
29. Levine, H.; Schwinger, J. On the theory of electromagnetic wave diffraction by an aperture in an infinite plane conducting screen. *Commun. Pure Appl. Math.* **1950**, *3*, 355–391. [CrossRef]
30. Taleb, S.I.; Neipp, C.; Francés, J.; Martínez Guardiola, F.J.; Alvarez, M.L.; Márquez, A.; Gallego, S.; Beléndez, A. 2D Green's tensor for the analysis of dielectric structures with translational geometries. In *Optics, Photonics and Lasers: Proceedings of the 4th International Conference on Optics, Photonics and Lasers (OPAL' 2021), 13-15 October 2021, Curfu, Greece*; International Frequency Sensor Association (IFSA) Publishing: Barcelona, Spain, 2021.
31. Yaghjian, A.D. Electric dyadic Green's functions in the source region. *Proc. IEEE* **1980**, *68*, 248–263. [CrossRef]